

# Chemical discontinuity at the extratropical tropopause and isentropic stratosphere-troposphere exchange pathways diagnosed using Aura MLS data

J. J. Jin,<sup>1,3</sup> N. J. Livesey,<sup>1</sup> G. L. Manney,<sup>1,2,4</sup> J. H. Jiang,<sup>1</sup> M. J. Schwartz,<sup>1</sup> and W. H. Daffer<sup>1</sup>

Received 12 August 2012; revised 10 February 2013; accepted 21 February 2013; published 13 May 2013.

[1] The chemical discontinuity at the extratropical tropopause (ExTP) and stratosphere-troposphere exchange (STE) pathways are investigated using the long-lived chemical species carbon monoxide (CO) and ozone ( $O_3$ ) measured by the Aura Microwave Limb Sounder (MLS). A relative coordinate, tropopause latitude (TpLat), is developed based on potential vorticity (PV) from the Goddard Earth Observing System version 5 (GEOS-5) data assimilation system. TpLat is defined as the shortest geographic distance along an isentropic surface from the extratropical tropopause (ExTP) to an observation location. Our results show that this coordinate highlights the sharp chemical discontinuities at the ExTP more clearly than the widely-used equivalent latitude coordinate. Geographical distributions of STE pathways and barriers are investigated based on meridional gradients in  $O_3$  abundances in the new TpLat coordinate in conjunction with analysis of Rossby wave breaking between 330 K and 360 K. In northern hemispheric (NH) winter (Dec–Jan–Feb), NH STE pathways are seen mainly above the northeast Pacific. In NH summer (Jun–Jul–Aug), the NH pathway covers all longitudes at 330 K. However, it is mainly located above Asia at 340 K and above the Atlantic and the North Pacific at 350 K and 360 K. In the southern hemisphere (SH), there is a weaker STE region above the Eastern Indian Ocean and the southwestern Pacific, at and above 350 K in SH winter, and a stronger STE region over the Southeastern Pacific at these levels during SH summer. In addition, this study shows NH PV gradients are slightly stronger near the ExTP in summer than in winter even though the subtropical jet is weaker and Rossby wave breaking is stronger in summer than in winter.

**Citation:** Jin, J. J., N. J. Livesey, G. L. Manney, J. H. Jiang, M. J. Schwartz, and W. H. Daffer (2013), Chemical discontinuity at the extratropical tropopause and isentropic stratosphere-troposphere exchange pathways diagnosed using Aura MLS data, *J. Geophys. Res. Atmos.*, 118, 3832–3847, doi:10.1002/jgrd.50291.

## 1. Introduction

[2] Stratosphere-troposphere exchange (STE) has been a topic of considerable research interest [e.g., Holton *et al.*, 1995; Stohl *et al.*, 2003; Fueglistaler *et al.*, 2009; Gettelman *et al.*, 2011, and references therein]. STE impacts atmospheric constituents such as ozone ( $O_3$ ) and water vapor ( $H_2O$ ) in the upper troposphere and lower stratosphere (UTLS). These trace

gases play an important role in the radiative balance of the UTLS and in surface temperature change [e.g., Hegglin and Shepherd, 2009; Solomon *et al.*, 2010]. The main STE pathways involve ascent of tropospheric air in the tropics and descent of stratospheric air in the extratropics through the Brewer-Dobson circulation. Rossby wave breaking (RWB) in the subtropics and two-way adiabatic transport between the UT and the LS are also important STE mechanisms [e.g., Holton *et al.*, 1995; Stohl *et al.*, 2003, and references therein]. Vertical mixing between isentropes near the tropopause has been shown to play an important role in STE on short-time scales [Hegglin *et al.*, 2005]. The net mass flux from the stratosphere to the troposphere in the extratropics is larger in winter than in summer [Appenzeller *et al.*, 1996a; Sprenger and Werli, 2003; Schoeberl, 2004]. However, episodic STE events such as deep stratospheric and troposphere intrusions [Appenzeller *et al.*, 1996b; Bithell *et al.*, 1999; Waugh and Funatsu, 2003] occur more frequently in summer than in winter because of weaker subtropical jets and stronger RWB near the extratropical tropopause (ExTP) during summer than during winter [Postel and Hitchman, 1999; Hitchman and Huesmann, 2007; Ndarana and Waugh, 2011]. These STE

Additional supporting information may be found in the online version of this article.

<sup>1</sup>Jet Propulsion Laboratory, California Institute of Technology, Pasadena, California, USA.

<sup>2</sup>New Mexico Institute of Mining and Technology, Socorro, New Mexico, USA.

<sup>3</sup>Now at GESTAR, Universities Space Research Association, Columbia, Maryland, USA.

<sup>4</sup>Now at NorthWest Research Associates, Socorro, New Mexico, USA.

Corresponding author: J. J. Jin, Global Modeling and Assimilation Office, Code 610.1, Goddard Space Flight Center, NASA, Greenbelt, MD, USA. (jianjun.jin@nasa.gov)

events have also been characterized through analysis of measurements of tracers such as carbon monoxide (CO), nitrous oxide ( $N_2O$ ),  $O_3$ , and  $H_2O$  [e.g., Pan et al., 2004; Ray et al., 2004; Hegglin et al., 2006; Olsen et al., 2008; Tilmes et al., 2010; Gettelman et al., 2011; Homeyer et al., 2011; Santee et al., 2011; Vogel et al., 2011, and references therein].

[3] A global view of the vertical distribution of tracer abundances is provided by Hegglin et al. [2009] using multiple-year satellite observations, and by Tilmes et al. [2010] using a large collection of aircraft measurements. In these, and many other, studies, a tropopause-referenced coordinate in the vertical direction [Logan, 1999; Birner et al., 2002; Pan et al., 2004; Birner, 2006] is employed. In views on isentropic surfaces that cut through both the troposphere and stratosphere, trace gas abundances show large meridional gradients at the location of the ExTP, reflecting the horizontal chemical discontinuities at the ExTP [Hegglin et al., 2006; Strahan et al., 2007; Kunz et al., 2011a; Santee et al., 2011, and references therein].

[4] The large vertical and horizontal chemical discontinuities at the ExTP reflect dramatic changes in atmospheric dynamical conditions. There are sharp increases in potential vorticity (PV) with altitude and latitude at the location of the ExTP [Hoskins et al., 1985; Ambaum, 1997; Martius et al., 2010], associated with the rapid increase of static stability at the tropopause [Birner, 2006; Randel et al., 2007; Hegglin et al., 2009; Grise et al., 2010]. These sharp horizontal PV gradients at the ExTP result in small effective diffusivity and Lyapunov diffusivity, two diagnostics of atmospheric mixing, at the ExTP [Haynes and Shuckburgh, 2000b; Shuckburgh et al., 2009], indicating a barrier to the mixing of air between the troposphere and the stratosphere that maintains the differences in chemical tracer abundances between the UT and the LS.

[5] There are large regional variations in the chemical discontinuity at the ExTP [Kunz et al., 2011a]. Shuckburgh et al. [2009] show that there are large geographical and seasonal variations in the small Lyapunov diffusivity at the ExTP. In addition, Shuckburgh et al. [2009] and Kunz et al. [2011a] show correlation between these variations and variations in RWB [e.g., Postel and Hitchman, 1999; Hitchman and Huesmann, 2007; Ndaramana and Waugh, 2011]. Large diffusivities and weak discontinuities in chemical tracers are located in regions with strong RWB, while small diffusivities and large meridional gradients in tracers are located in regions with quiescent RWB. Therefore, the chemical discontinuity is directly related to the STE process: Large discontinuities represent weak STE at the ExTP, indicating that the ExTP is a transport barrier [Haynes and Shuckburgh, 2000b; Shepherd, 2002; Berthet et al., 2007; Santee et al., 2011] while regions with weak discontinuities are STE pathways.

[6] In this study, the chemical discontinuity at the ExTP is investigated, and STE pathways and barriers are discussed. A new tropopause coordinate is developed in order to closely characterize the fine structure of the ExTP. This study, in general, extends the approach of Kunz et al. [2011a]. A relative tropopause equivalent latitude (TpEqLat, hereafter) coordinate, based on a new definition of the ExTP [Kunz et al., 2011b], is introduced by Kunz et al. [2011a], and the chemical and dynamical discontinuities at the ExTP are discussed in their study. However, sorting measurements

or model data according to PV values by mapping with respect to dynamical equivalent latitude (EqLat) [Butchart and Remsberg, 1986; Hegglin et al., 2006] alters the view at the ExTP [Manney et al., 2011; Pan et al., 2012] because in the UTLS, there is not a single simply connected jet and associated region of strong PV gradients defining a transport barrier that separates air masses as there typically is in the stratosphere. In this study, a new relative coordinate is introduced, where EqLat is replaced with geographic distance. Tropospheric and stratospheric measurements or model analyses are arranged with respect to the varying ExTP geographical locations in the new coordinate (see more details in section 3). This new coordinate provides a means not only to account for the reversible transport between the UT and LS as does the TpEqLat coordinate but also to provide a clearer view of fine atmospheric structures at the ExTP than does the TpEqLat coordinate.

[7] Section 2 of this paper provides a description of Aura Microwave Limb Sounder (MLS) CO and  $O_3$  measurements [Livesey et al., 2011], and the Goddard Earth Observing System version 5 (GEOS-5) meteorological data [Rienecker et al., 2008], the two datasets used in this study. Section 3 provides details on the new tropopause coordinate and the chemical discontinuity at the ExTP seen by Aura MLS. In section 4, regional variations in STE pathways and barriers are investigated by analyzing MLS measurement distributions in the new coordinate and RWB activities near the ExTP. Discussion and summary are provided in section 5.

## 2. Aura MLS CO and $O_3$ Measurements and GEOS-5 Data

### 2.1. MLS CO and $O_3$

[8] Microwave Limb Sounder version 3 [Livesey et al., 2011] CO and  $O_3$  measurements are analyzed in this study. Tropospheric CO is produced through incomplete combustion of fossil fuels and biomass in the boundary layer and from oxidation of methane ( $CH_4$ ) and non-methane hydrocarbons in the free troposphere. CO volume mixing ratios (VMRs) generally decrease with altitude in the troposphere and LS. In the middle and upper stratosphere, CO is mainly produced from the oxidation of  $CH_4$ . It is destroyed through the reaction with hydroxyl radicals (OH) in the troposphere and stratosphere. Its chemical lifetime is about 2 to 6 months in the UTLS region, which is comparable to the large-scale slow ascent time scale (about 1 km per month) near the tropical tropopause but is longer than the typical advection and mixing time scales in the subtropics and mid-latitudes. Therefore, CO is useful as a tracer of atmospheric motions [e.g., Allen et al., 1999; Schoeberl et al., 2006; Jin et al., 2009, and references therein] and for STE processes [e.g., Pan et al., 2004; Hoor et al., 2010].

[9]  $O_3$  is produced in both the troposphere and the stratosphere through photochemistry. However, its production is much larger in the stratosphere than in the troposphere.  $O_3$  abundances increase abruptly from tens of ppbv (part per billion in volume) in the UT to hundreds of ppbv in the LS. It has a long chemical lifetime, of the order of months, in the UTLS region. Therefore,  $O_3$  is also widely used as a tracer in STE studies [e.g., Fischer et al., 2000; Pan et al., 2004; Gettelman et al., 2011; Santee et al., 2011, and references therein]. The different character of the CO and  $O_3$  distributions

in the UTLS enables irreversible mixing between tropospheric and stratospheric air masses to be diagnosed: Large CO and small O<sub>3</sub> abundances are seen in air of tropospheric origin, while air parcels originating in the stratosphere have large O<sub>3</sub> and small CO abundances. Simultaneous measurements of the two species give insights on troposphere-to-stratosphere transport and stratosphere-to-troposphere transport [e.g., Fischer *et al.*, 2000; Hoor *et al.*, 2002, 2010; Stohl *et al.*, 2003; Pan *et al.*, 2004] and on the structure of the ExTP [Hegglin *et al.*, 2009].

[10] Microwave Limb Sounder retrievals are made on pressure surfaces. The vertical resolution of the measurements is about 3–5 km in the UTLS. Preliminary validation shows that the factor of 2 positive bias at 215 hPa in MLS version 2 CO data [Livesey *et al.*, 2008] has been significantly reduced in version 3, while the observed morphology is retained (albeit with a slight increase in noise) [Livesey *et al.*, 2011]. MLS version 3 CO measurements made at 215 hPa, 147 hPa, and 100 hPa are used in this study. The vertical retrieval grid for MLS version 3 O<sub>3</sub> is twice as fine as that used in the MLS CO retrievals, and five O<sub>3</sub> levels from 215 hPa to 100 hPa are used in this study. This study considers the MLS measurements made between August 2004 and December 2011.

## 2.2. GEOS-5 Data

[11] The Goddard Earth Observing System Version 5 (GEOS-5) [Rienecker *et al.*, 2008] is a data assimilation system based on a coupled atmosphere and ocean global circulation mode with other components including land surface model and sea ice model. A finite-volume dynamical core [Lin, 2004] is employed in the GEOS-5, which has 72 hybrid sigma-pressure layers between the surface and 0.01 hPa. The horizontal resolution is 1/2 degree latitude × 2/3 degree longitude. The vertical resolution is about 1 km in the UTLS region. Wind, temperature, moisture, cloud, radiance, and O<sub>3</sub> measurements are assimilated into GEOS-5 using a 6 h time window. The four daily analyses are used to compute incremental analysis updates [Bloom *et al.*, 1996] for the assimilated fields. Following Pawson *et al.* [2007], 6 h averaged wind and PV fields are used in this work.

[12] The GEOS-5 version v5.1 and v5.2 results are used to aid interpretation of MLS observations between August 2004 to September 2008 and after September 2008, respectively. Although the GEOS-5 analysis fields show large deficiencies in the upper stratosphere and lower mesosphere [e.g., the stratopause region during sudden stratospheric warmings; Manney *et al.*, 2008], GEOS-5 DAS fields in the UTLS are well constrained by observations and provide reliable meteorological analyses.

## 3. Tropopause Latitude Coordinate (TpLat) and Chemical Discontinuity at the ExTP

### 3.1. TpLat Coordinate

[13] In this section, a tropopause latitude coordinate (TpLat) is developed that will be shown to be useful in describing climatological features of the extratropical tropopause. On a given isentropic surface, TpLat is the distance to the closest point at which the tropopause intersects the

surface and is represented in Figure 1 (top panel) by green and purple contours in the UT and LS, respectively. In other words, TpLat is the horizontal distance from the nearest ExTP, independent of whether that is the main ExTP or a “secondary” ExTP that arises via RWB [Postel and Hitchman, 1999; Hitchman and Huesmann, 2007; Ndarama and Waugh, 2011], to the observation location. The geographic distances are transformed to latitudinal degrees using a mean Earth radius 6370 km. This study uses the 3.5 or –3.5 PVU (standard PV unit; 1 PVU = 10<sup>-6</sup> K m<sup>2</sup> kg<sup>-1</sup> s<sup>-1</sup>) isoline tropopause [Hoerling *et al.*, 1991; Schoeberl, 2004] in the NH or SH extratropics and the 380 K (potential temperature) tropopause in the tropics between the latitudes where the PV isoline meets the 380 K surface. Tropospheric and stratospheric locations correspond to small (less than 3.5 PVU) and large (greater than 3.5 PVU) absolute PV values. In the NH, TpLat is defined to be negative for a tropospheric location, and positive for a stratospheric location, independent of whether the location is on the equatorward or poleward side of the tropopause. This sign convention is inverted for a location in the SH.

[14] Previous studies have employed other tropopause definitions in addition to traditional temperature lapse rate definition [World Meteorological Organization, WMO, 1995] and dynamical tropopause definition based on a particular potential vorticity (PV) value [e.g., Holton *et al.*, 1995]. For example, a particular O<sub>3</sub> value (e.g., 100 ppbv) has been used for separating stratospheric air from tropospheric air [Berhan *et al.*, 1996; Hsu *et al.*, 2005]. Zahn and Breininkmeijer [2003] and Pan *et al.* [2004] define a “chemical tropopause” in the extratropics using the correlation of the stratospheric tracer O<sub>3</sub> and the tropospheric tracer carbon monoxide (CO). Prather *et al.* [2011] recently proposed the use of “model e90 tropopause”, determined by the abundance of an artificial model tracer with surface sources and a 90 day decay time. The tropopause can also be defined in terms of a sharp change in the probability that an air parcel has been in the boundary layer within a given time [Berthet *et al.*, 2007]. Kunz *et al.* [2011b] define the extratropical dynamical tropopause location at the EqLat of the maximum in the product of the meridional PV gradient with respect to EqLat and the horizontal wind speed on an isentropic surface. This tropopause definition is used in their follow-up study in the chemical and dynamical discontinuities [Kunz *et al.*, 2011a]. Prior to that study by Kunz *et al.* [2011b], Polvani and Esler [2007] define the extratropical dynamical tropopause to be at the location of the maximum meridional PV gradient with respect to geographic latitude on an isentropic surface, consistent with the original concept of dynamical tropopause [Reed, 1955].

[15] For this study, a PV-based dynamical tropopause definition has been chosen. Various PV values ranging between 1.5 PVU and 5 PVU have previously been employed to define the tropopause [e.g., Haynes and Shuckburgh, 2000b; Highwood *et al.*, 2000; Scott *et al.*, 2003; Pan *et al.*, 2004, 2007; Schoeberl, 2004; Krebsbach *et al.*, 2006; Santee *et al.*, 2011]. Figure 2 shows NH seasonal mean “meridional” gradient in GEOS-5 PV in the newly defined TpLat coordinate around the ExTP between 330 K and 370 K (about 12–17 km) in Dec–Jan–Feb (DJF) and Jun–Jul–Aug (JJA). As stated above, 0° TpLat is the location of the ExTP. In this figure, PV values of 2.0 PVU, 3.5 PVU, and 5.0 PVU are examined

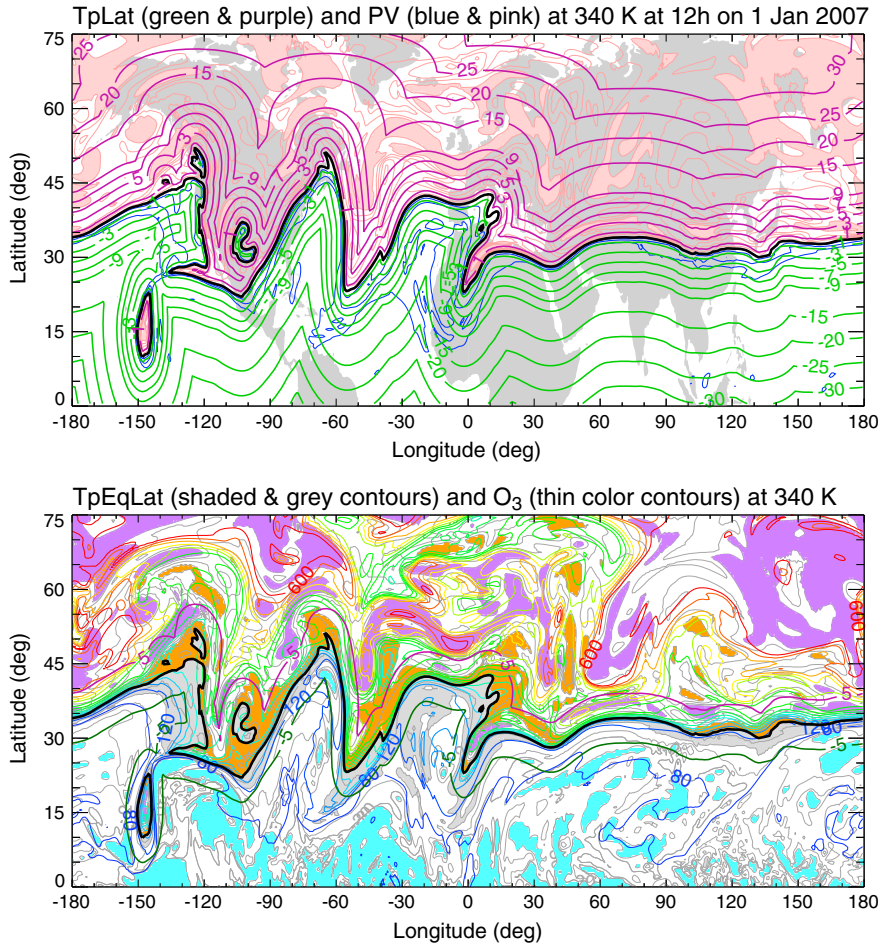


**Figure 1.** (Top) A map of TpLat (purple contours for positive values, and green contours for negative values), GEOS-5 potential vorticity (PV; blue contours: 1, 2, and 3 PVU; and pink contours: 4, 5, 6, 7, and 8 PVU; pink areas, PV > 8 PVU), and locations of the extratropical tropopause (ExTP, black curves and contours). TpLat is defined as the geographic distances from the nearest tropopause locations to the observation locations on an isentropic surface, and its unit is latitudinal degree. (Bottom) A map of TpEqLat (grey contours at  $-30^{\circ}$ ,  $-20^{\circ}$ ,  $-10^{\circ}$ ,  $-5^{\circ}$ ,  $5^{\circ}$ ,  $10^{\circ}$ ,  $20^{\circ}$ , and  $30^{\circ}$  and shaded), and GEOS-5 ozone (color contours between 80 and 600 ppbv with an interval of 40 ppbv). TpEqLat less than  $-30^{\circ}$ , between  $-5^{\circ}$  and  $0^{\circ}$ , between  $0^{\circ}$  and  $5^{\circ}$ , and greater than  $30^{\circ}$  are shaded in cyan, grey, orange, and purple, respectively. Locations of the ExTP and  $-5^{\circ}$  and  $5^{\circ}$  TpLat are also shown in the bottom map. Here, the tropopause is the 3.5 PVU isoline dynamical tropopause in the extratropics. Tropospheric TpLat and TpEqLat (negative in the NH) and stratospheric TpLat and TpEqLat (positive in the NH) are determined by small ( $<3.5$  PVU) and large ( $>3.5$  PVU) absolute PV values, respectively. See section 3 for more details.

to determine which is the most appropriate ExTP ( $0^{\circ}$  TpLat) PV threshold. It is evident that the largest “zonally” and seasonally averaged meridional gradients in PV occur at or very close to the location of the ExTP for all of the three dynamical tropopause definitions. In general, variations of the maximum meridional gradients in PV are small in DJF. In JJA, these values at the ExTP are larger for 3.5 PVU and 5.0 PVU tropopause definitions than the maximum gradients based on 2.0 PVU tropopause definition. The 3.5 PVU contour appears to be near the center to the band of enhanced PV gradient around the ExTP, so it has been adopted for use in the definition of TpLat. This choice is in accord with Hoerling *et al.*, 1991, Schoeberl [2004] and Gettelman *et al.* [2011], who demonstrate that the thermal tropopause roughly corresponds to the 3.5 PV isoline at middle latitudes.

[16] The TpLat coordinate is a modification of the TpEqLat coordinate introduced by Kunz *et al.* [2011a]. In addition to the difference in tropopause definitions between this study and the study conducted by Kunz *et al.* [2011a], there is a fundamental difference in calculating distances between measurement or analysis locations and the ExTP: These distances are calculated in EqLat for the EqTpLat coordinate, but in geographic distance for the new TpLat coordinate. EqLat is a dynamical coordinate defined as the latitude that encloses the same area between it and the pole as a given potential vorticity contour [Butchart and Remsberg, 1986; Hegglin *et al.*, 2006]. Thus, the zonal variations in PV in geographical coordinates are removed when viewed with respect to EqLat. The EqLat coordinate is a powerful tool for studying stratospheric chemical tracer

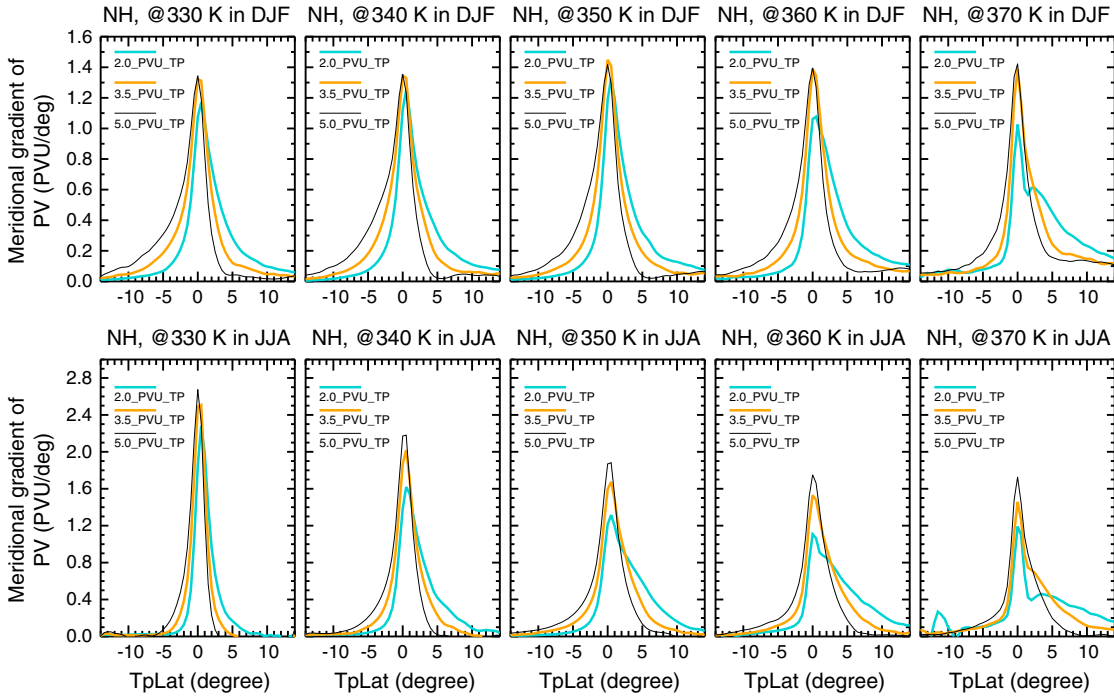


**Figure 2.** Northern hemispheric seasonal mean meridional gradients in GEOS-5 PV in TpLat coordinates at 330 K–370 K in Dec–Jan–Feb (DJF, upper panels) and Jun–Jul–Aug (JJA, bottom panels). Different tropopause PV values are used to find the most appropriate tropopause ( $0^{\circ}$  TpLat) PV threshold. Note that ranges of the y axis scale are larger in the bottom panels than in the upper panels. These results are derived from GEOS-5 PV fields in year 2007.

distributions and evolution for precisely this reason [e.g., Manney *et al.*, 1999, 2007, 2009, 2011, and references therein] since PV values typically increase monotonically toward the center of a polar vortex defined by a single, simply connected jet. In the UTLS, however, the jets are typically complex and discontinuous [Manney *et al.*, 2011; Manney *et al.*, 2013, *Climatology and Variability of Upper Tropospheric/Lower Stratospheric (UTLS) Jet from MERRA, paper in preparation, hereafter M2013*], and associated with multiple large (large negative in the SH) PV centers (Figure 1, top panel). Air near the middle latitude tropopause but with large PV values, e.g., air located in the shaded areas near the ExTP in Figure 1 (top panel), would be located at high equivalent latitudes in EqLat coordinate (Figure 1, bottom panel). Therefore, characterizing tracer distributions around the ExTP using EqLat can introduce biases [Manney *et al.*, 2011; Pan *et al.*, 2012]. The advantage of TpLat compared to TpEqLat is further demonstrated later in this section.

[17] Since the subtropical jet plays an important role in defining the structure of the ExTP, Manney *et al.* [2011] introduced a coordinate system relative to the jet cores in horizontal and vertical directions for studying transport in the UTLS. A jet core is defined using their method where the wind speed in it is greater than 40 m/s. This “jet coordinate” may thus not be defined where the jet is weak, which is not uncommon during summer. Although the dynamical tropopause is not well defined in tropics, it is virtually always well defined in the extratropics. Therefore, TpLat can be a complementary tool to the jet coordinate. A discussion of the relationship between TpLat and the jet coordinate is provided below and in section 5.

### 3.2. Chemical Discontinuity at the ExTP

[18] To further investigate the difference between TpLat and the widely-used TpEqLat (or EqLat) coordinate, Figure 3 shows the TpLat and TpEqLat values for NH MLS observations between  $340 \pm 5$  K on 3–5 May in 2005 through 2011 with colors representing (a) GEOS-5 PV, (b) MLS CO, (c) GEOS-5 horizontal wind speeds, and (d) MLS O<sub>3</sub> values at these MLS locations. The same PV value (3.5 PVU) is used to determine tropopause locations in TpLat and TpEqLat coordinates; thus, these TpLat and TpEqLat are drawn from the same ensemble of ExTP locations. However, PV distributions in the UTLS are different in the two coordinates: They are compact in the TpEqLat coordinate while scattered in the TpLat coordinate. This is not surprising, since PV is aligned with EqLat by definition, while only the 3.5 PV contour is defined to be aligned with TpLat.

[19] Dramatic changes in CO and O<sub>3</sub> abundances between the UT and the LS are apparent in both coordinates (Figures 3b and 3d). However, their distributions are different near the ExTP. High CO and low O<sub>3</sub> values geographically near the ExTP are spread out in the UT in the TpEqLat coordinate. This wide separation in O<sub>3</sub> abundances in TpEqLat is because of the large range of PV values near the ExTP. Moreover, the large spread of CO and O<sub>3</sub> in the LS is likely partially due to strong adiabatic mixing in addition to being related to the coarse vertical resolution in the MLS observations. This is supported by strong intersections between GEOS-5 TpEqLat (PV or EqLat) and GEOS-5 O<sub>3</sub> [Wargan *et al.*, 2010] contours even though high O<sub>3</sub> values are, in general, aligned with large TpEqLat contours as shown in Figure 1 (bottom panel).

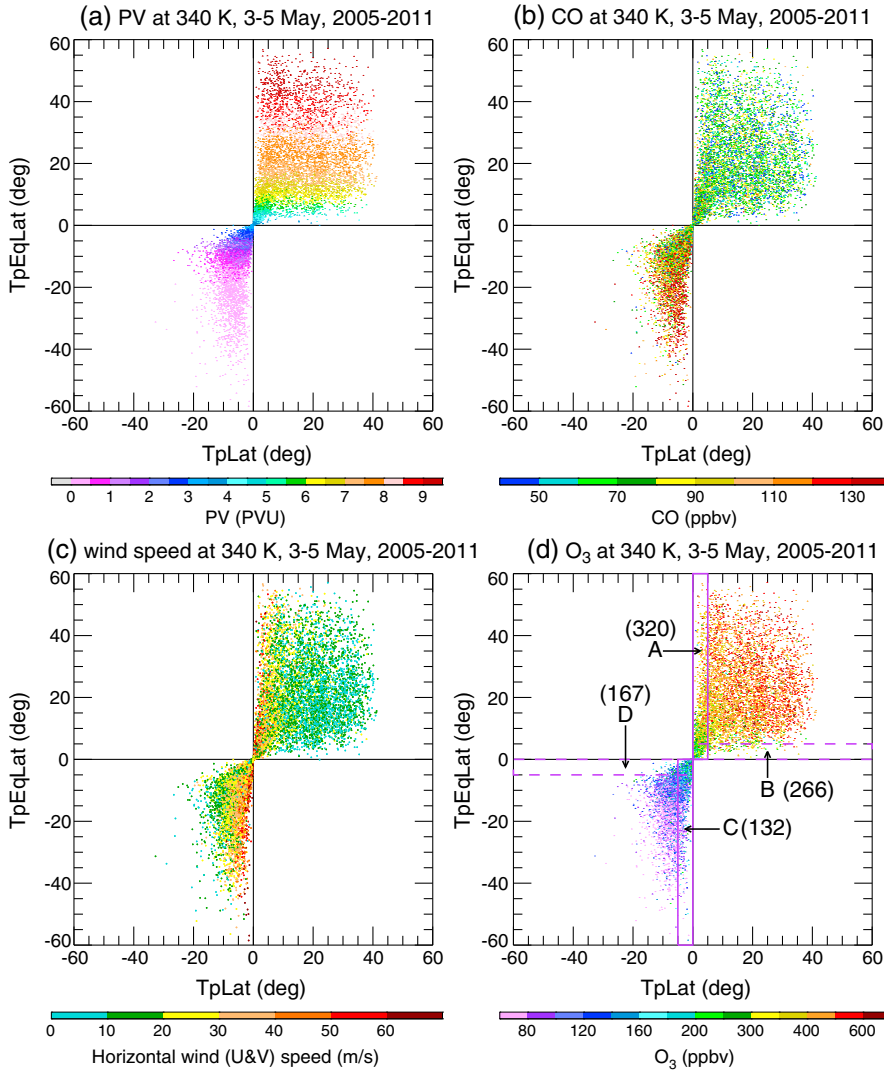


**Figure 3.** TpLat and TpEqLat for NH MLS observations at 340 K on 3–5 May, 2005–2011. Individual point colors represent (a) GEOS-5 PV, (b) MLS CO, (c) GEOS-5 horizontal wind speeds, and (d) MLS O<sub>3</sub> values. In Figure 3d, locations between 0° and 5° TpLat, and between −5° and 0° TpLat are bounded in purple solid-line rectangles A and C, respectively. Locations between 0° and 5° TpEqLat, and between −5° and 0° TpEqLat are bounded in purple dashed-line rectangles B and D, respectively. Numbers in parentheses are mean O<sub>3</sub> abundances inside the narrow rectangles A, B, C, and D.

[20] Figure 3d shows mean O<sub>3</sub> values in LS and UT at locations within 5° of the tropopause in TpLat and in TpEqLat (bounded by rectangles). These mean values, 167 ppbv and 132 ppv within −5° to 0° in TpEqLat and TpLat coordinate, respectively, are larger than O<sub>3</sub> values previously considered characteristic of the UT [e.g., 100 ppbv or less; e.g., Pan *et al.*, 2004; Hegglin *et al.*, 2009]. This may be due to the application of the 3.5 PVU ExTP threshold, which may lead to a slight stratospheric mislocation of the ExTP at 340 K. Supplementary Figure S1 in the auxiliary material shows that these mean O<sub>3</sub> abundances are close to 100 ppbv in the UT when a 2 PVU tropopause threshold is used. We note that the difference between O<sub>3</sub> values in the UT and the LS is significantly larger in the TpLat coordinate than in the TpEqLat coordinate. This is because of the large range of EqLat that is geographically near the ExTP as discussed above. In addition, distances in EqLat are not identical to

geographic distances and 0° to 5° (−5°) TpLat covers more stratospheric (tropospheric) area than 0° than 5° (−5°) TpEqLat (Figure 1, bottom map). Nevertheless, this suggests that the dynamical TpEqLat coordinate cannot completely capture the abruptness of the changes in chemical tracers at the ExTP.

[21] Figure 3c shows GEOS-5 horizontal wind speeds at MLS observation locations. Although winds are strong near the ExTP in both views, the morphologies are different in the two coordinates. The figure shows extremely strong winds near 0° TpLat that weaken with increasing TpEqLat distance from the ExTP. However, there is not a monotonic relationship between wind speeds and TpEqLat distance from the ExTP. Previous studies have demonstrated that the ExTP is generally co-located with the jet core at about 340 K–350 K and winds weaken with distance from the ExTP [e.g., Manney *et al.*, 2011; Kunz *et al.*, 2011b]. Clearly, TpLat is much

better than TpEqLat in depicting the UTLS wind structure, consistent with the results of *Manney et al.* [2011] showing that a jet coordinate (which corresponds closely to the TpLat coordinate in all regions where a jet is defined) captures the wind variations more completely than an EqLat coordinate.

[22] This figure also confirms that the ExTP can be accurately located using combined wind velocity and PV gradient information as proposed by *Kunz et al.* [2011b]. However, we reemphasize that the fundamental difference between our TpLat and the TpEqLat developed by *Kunz et al.* [2011a] is in measuring the distances from the tropopause in geographic distance versus EqLat, rather than in the method used to identify the tropopause itself.

[23] Concerns about the TpLat coordinate may arise for measurements that are located far away from the tropopause but have PV values close to 3.5 PVU, as shown by some measurements with large positive and negative TpLat values near  $0^\circ$  TpEqLat. EqLat values are derived through calculating areas enclosed by PV contours on isentropic surfaces as stated above. Data with absolute PV values close to 3.5 PVU have EqLat values close to that of the ExTP, whether they are horizontally or vertically near the ExTP. In TpLat coordinate, only horizontal distances are counted in TpLat distances, and some data are located far away from the ExTP even though they are vertically near the tropopause below or above them and have absolute PV values close to 3.5 PVU.

[24] Figure 4 shows the evolution of multi-year (2004–2011) “zonal” mean CO and PV on 340 K and 360 K isentropic surfaces (about 13 km and 16 km, see Supplementary Figure S2 for CO and PV on the 330 K and 350 K isentropic surfaces) in the TpLat coordinate (left panels) and the TpEqLat coordinate (right panels). The climatological locations of the extratropical tropopause, represented by 3.5 PVU isolines,

are drawn as black curves in all of the panels. We note that this figure is produced by binning a large number of MLS observations over a potential temperature range of  $\pm 5$  K ( $\sim 0.5$  km in the UTLS region) around the stated level instead of vertically interpolating from the MLS pressure levels since interpolating these measurement, which have coarse vertical resolution (about 3 km), can smoothen the sharp transition in the UTLS more than binning them within a smaller altitude range (about 1 km) does. The bin size is  $2^\circ$  latitude TpLat/TpEqLat, and temporal bin size is 3 days. Bins with fewer than 10 measurements are considered to be missing data (shown as white space).

[25] One striking feature shown in Figure 4 is the sharp distinction between both CO abundances and PV values in the UT compared to those in the LS at all of these levels in both TpLat and TpEqLat coordinates, demonstrating the chemical and dynamical discontinuities at the ExTP ( $0^\circ$  TpLat/TpEqLat), as shown by *Kunz et al.* [2011a] for the TpEqLat coordinate. High CO abundances are seen in the UT during spring and summer in both TpLat and TpEqLat coordinates. This is mainly related to the outflow of North American and Asian CO [e.g., *Li et al.*, 2005; *Fu et al.*, 2006; *Jiang et al.*, 2007; *Park et al.*, 2009; *Randel et al.*, 2010]. Increased CO abundances are also seen at 340 K in the LS during this period, although these are much smaller than the abundances in the UT in those seasons.

[26] Closely spaced GEOS-5 PV contours are seen at the location of the ExTP. In TpEqLat coordinate, the PV contours are aligned with the ExTP, by definition, before temporal averaging is performed. However, this alignment is not guaranteed in TpLat coordinate, as indicated by large longitudinal variations of PV values along the ExTP in Figure 1 and discussed above. Nevertheless, the sharp meridional gradient of PV values at the ExTP on short-time scales [e.g., *Hoskins et al.*, 1985; *Ambaum*, 1997; *Martius et al.*,

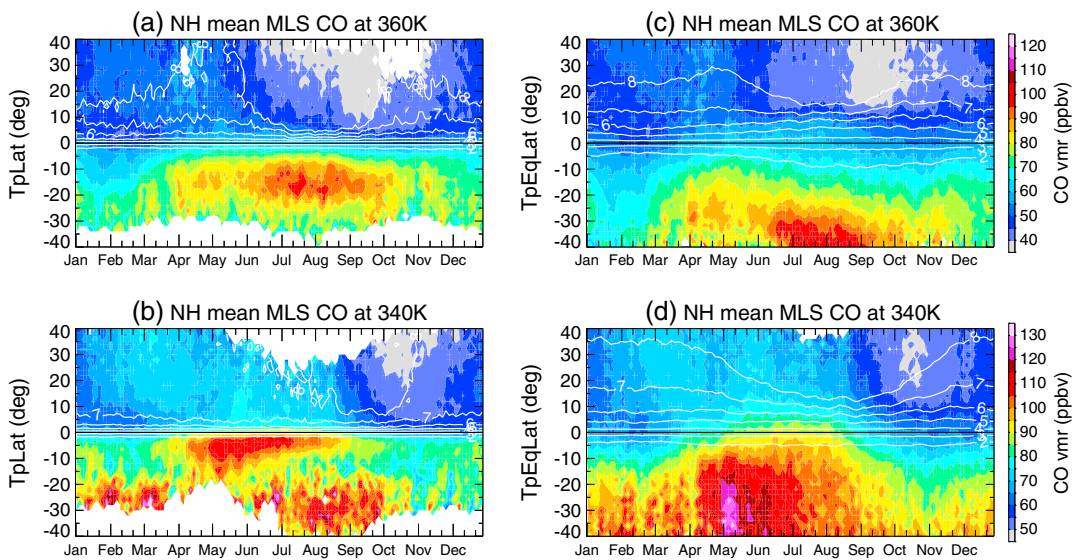


**Figure 4.** Evolution of NH “zonal” mean MLS CO (color with color bars on the most right) and GEOS-5 PV (white contours) at the 340 K and 360 K (within  $\pm 5$  K range) isentropic surface in TpLat coordinates (left panels) and TpEqLat coordinates (right panels). Black lines show locations of the tropopause. This figure shows MLS measurements made during 2004–2011, and blank areas represent regions where the number of measurements is fewer than 10. GEOS-5 PV values are sampled at MLS measurement locations before being averaged.

2010] is preserved in multi-year global means in both TpLat and TpEqLat coordinates. This all-season large PV gradient at the tropopause is consistent with the analysis of Birner [2006] who showed that the meridional PV gradient is related to the meridional gradients of static stability, which is large at the extratropical tropopause in all seasons [e.g., Randel et al., 2007; Hegglin et al., 2009; Grise et al., 2010; Gettelman et al., 2011].

[27] Figure 4 demonstrates that the multi-year mean chemical and dynamical discontinuities at the ExTP are larger in TpLat coordinate than those seen in TpEqLat coordinates as discussed above. The PV contours are more compact near the ExTP in TpLat coordinate (left panels) than in TpEqLat (right panels). During spring and summer, the decrease in CO abundances at the ExTP in the TpLat coordinate is more sudden than that in the TpEqLat coordinate at both isentropic levels. UT air with high CO abundances is found near the ExTP, especially at 340 K, during spring and summer in the TpLat coordinate. This is consistent with the large vertical outflow of surface air pollution in middle-latitude East Asia and North America during the two seasons [Li et al., 2005; Jiang et al., 2007]. However, these high tropospheric CO abundances are far away from the ExTP in the TpEqLat coordinate, resulting in smaller CO abundances near the ExTP compared to the values in TpLat coordinates. In short, the chemical and dynamical discontinuities at the ExTP, on a global and climatological scale, are significantly stronger than those reported using the TpEqLat coordinate [Kunz et al., 2011a].

[28] The smaller CO abundances near the ExTP and larger CO far from the ExTP at 340 K in the TpEqLat coordinate during spring-summer can be misleading because of the relocation of measurements in EqLat coordinates. Figure 3 reveals, for example, that most of the measurements with large CO VMRs but far away from the extratropical tropopause in the TpEqLat coordinate (e.g.,  $-40^{\circ}$ – $20^{\circ}$  TpEqLat, shown in Figure 3b) are geographically near the extratropical tropopause in early May. As stated above, high CO VMRs in the UT arise from fast vertical transport in the outflow of deep convection and in warm conveyor belts (WCBs) that are found ahead of the cold fronts associated with a cyclone [Stohl, 2001; Wernli and Bourqui, 2002]. Diabatic ascent in WCB outflow can reduce PV to very small values (0–0.5 PVU) in the UT and form a low PV streamer near the ExTP [Pomroy and Thorpe, 2000; Grames et al., 2011]. These small PV values correspond to low EqLat as shown in Figure 3a. As a result, air with high CO abundances and small PV values is artificially placed away from the ExTP in EqLat coordinates. This relocation not only reduces the chemical discontinuity at the ExTP but also distorts the CO distribution in the UT.

[29] However, Figure 4 demonstrates that TpEqLat is a useful tool for studying diabatic mixing and transport in the UTLS. The enhancement in CO abundance in the LS from spring to summer is due to irreversible troposphere-to-stratosphere transport in these seasons [e.g., Chen, 1995; Sprenger and Wernli, 2003; Hoor et al., 2010]. The diabatic STE is more evident in the right panels than in the left panels, suggesting TqEqLat is better at revealing diabatic mixing than the TpLat coordinate. Nevertheless, chemical distributions in the UTLS can be distorted by using EqLat as discussed above. Caution is needed when viewing them

in TpEqLat or EqLat as discussed in this study and by Manney et al. [2011] and Pan et al. [2012].

## 4. Geographical Distributions of STE Pathways and Barriers Seen by MLS and GEOS-5

### 4.1. Rossby Wave Breaking Identification

[30] The ExTP is a transport barrier [e.g., Holton et al., 1995; Haynes and Shuckburgh, 2000b; Shepherd, 2002; Berthet et al., 2007; Santee et al., 2011] in both vertical and horizontal directions that leads to large differences in tracer abundances in the UT and LS as discussed above. We note the transport barrier effect of the ExTP is not the sole factor for the distinction in tracer abundances between the UT and LS. As a typical example, the large difference between LS and UT CO is influenced by the CO source strength at the surface and through vertical transport in the troposphere. However, STE processes act to reduce the differences in tracer abundances between the two sides of the ExTP. In the horizontal, meridional gradients in tracer abundances are reduced by STE [Kunz et al., 2011a]. Therefore, the meridional gradient in a tracer's abundance is a good index of STE pathways and transport barriers if the tracer's distribution in the UTLS is mainly changed by STE. In this section, we investigate the regional and seasonal variations in STE pathways by analyzing MLS O<sub>3</sub> distributions and meridional gradients in MLS O<sub>3</sub> abundances in the tropopause latitude coordinate. MLS CO data are not used in this section because their geographical distribution in the UT is strongly influenced by CO emission on the surface [Li et al., 2005; Jiang et al., 2007].

[31] Previous studies have also shown STE is strongly influenced by RWB near the ExTP [Holton et al., 1995; Shepherd, 2002, and references therein]. Wernli and Sprenger [2007] developed a novel method for identifying tropospheric and stratospheric PV cutoff and streamer structures (see Figure 5) near the ExTP, which are influenced by RWB [Postel and Hitchman, 1999; Wernli and Sprenger, 2007, Hitchman and Huesmann, 2007; Ndarana and Waugh, 2011]. They quantified relationships between STE fluxes and RWB by simulating air parcel trajectories passing through these structures [Sprenger et al., 2007]. Using the method developed by Wernli and Sprenger [2007], we analyze RWB near the ExTP as represented in GEOS-5 PV and map this activity in the tropopause latitude coordinate. We thus present a combined analysis of chemical constituent distributions and RWB.

[32] Figure 5 highlights instantaneous GEOS-5 PV structures near the ExTP at 340 K on 1 Jan 2007. Areas shaded in cyan and orange are tropospheric and stratospheric cutoff PV structures, respectively. Areas shaded in blue and pink are tropospheric PV streamers (TrPV, hereafter) and stratospheric PV streamers (StPV, hereafter), respectively. While the identification of cutoff PV areas is unambiguous, the identification of PV streamers is empirical. Wernli and Sprenger [2007] define the streamers as areas bounded by the ExTP curves and the straight lines that start and end at the ExTP curves with lengths of the ExTP curve greater than 1500 km and straight lines lengths less than 800 km. Wernli and Sprenger [2007] also demonstrate the method reliably identifies RWB near the ExTP.

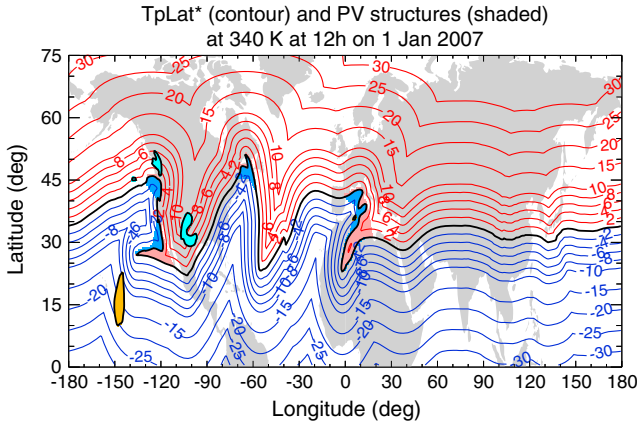


**Figure 5.** Same as the top map in Figure 1 but for TpLat\* (blue and red contours) and PV structures (shaded areas). TpLat\* is determined by the same way as TpLat illustrated in Figure 1 except that the ExTP around the cutoff PV regions (shaded in cyan and orange) are not used for determining TpLat\*. In the other words, all TpLat\* refer to the “main” ExTP. Areas shaded in orange and cyan represent tropospheric and stratospheric PV cutoff regions, respectively. Areas shaded in blue and pink represent tropospheric PV streamer (TrPV) regions and stratospheric PV streamer (StPV) regions, respectively. Cutoff PV, TrPV, and StPV regions are identified using the method developed by Wernli and Sprenger [2007]. See text for more details.

[33] In contrast to our earlier definition, in this section, the tropopause latitude coordinate (hereafter TpLat\*) is defined as the shortest distance from the “main” ExTP, the longest and simply connected 3.5 PVU ( $-3.5$  PVU) contour in the NH (SH) on a given isentropic surface, as shown in Figure 5. This means that the tropopause locations around the cutoff PV area (in cyan and orange) are ignored. We make this choice because our focus is on the STE pathway at the main ExTP. However, the occurrence frequency of these structures is shown in Figures 6, 7, and 8. This modification in the TpLat coordinate definition may reduce the meridional gradients in  $O_3$  abundance near the ExTP since the distance from the tropopause to some measurement locations that are near the cutoff PV structures will increase. However, this modification only has a small influence on the meridional gradients near the main ExTP (not shown) and does not significantly bias our analysis.

#### 4.2. STE Pathways and Barriers in the North Hemisphere

[34] Figure 6 shows the distribution of MLS  $O_3$  and its meridional gradients, which are the derivatives of  $O_3$  abundances with respect to TpLat\*, in the TpLat\* coordinate, and PDFs of NH PV structures in the NH winter season (DJF). Combined PDFs for TrPV and tropospheric cutoff PV structures (StPV and stratospheric cutoff PV structures) are shown as black (color) contours atop of geographical maps in the right panels, while PDFs for tropospheric and stratospheric cutoff PV structures and PV streamers (TrPV and StPV) in TpLat\* coordinate are shown in the left and middle panels, respectively. We note that PDFs for tropospheric (stratospheric) cutoff PV structures are plotted on

the stratospheric (tropospheric) side of the main ExTP (in the left panels) in order to make them align with their geographical relative locations with respect to the main ExTP.

[35] Figure 6 demonstrates strong regional variations in RWB near the ExTP [Postel and Hitchman, 1999; Wernli and Sprenger, 2007; Hitchman and Huesmann, 2007; Ndarana and Waugh, 2011]. Large PDF values of the PV structures suggest frequent RWB near the ExTP. It can be seen that the maximum PDF centers are located above the Eastern Pacific and the Eastern Atlantic in the subtropics and middle latitudes (right panels), suggesting that these places are the most likely wave-breaking regions between 330 K and 360 K. These findings from GEOS-5 are consistent with previous results from other datasets [e.g., Wernli and Sprenger, 2007; Hitchman and Huesmann, 2007]. Figure 6 shows that PDFs for tropospheric PV structures are nearly the same as PDFs for stratospheric PV structures, although the contours of tropospheric PV structures are slightly shifted north of the contours of stratospheric PV structures in maps as demonstrated by Wernli and Sprenger [2007]. That the tropospheric and stratospheric PV structures have PDFs with nearly the same magnitude is also reflected in the generally symmetric distribution of PDFs for PV streamers and cutoff structures on either side of the ExTP in TpLat\* coordinates in the left and middle panels, which also demonstrates strong regional variations in RWB.

[36] The middle panels in Figure 6 show that the PV streamers (TrPV and StPV) are generally located within  $\sim 300$  km ( $\sim 3^\circ$ , latitude) of the main ExTP. Since TpLat\* is based on the relative distances from the main ExTP, distributions of these PV structures in TpLat\* coordinate also demonstrate how far a PV streamer extends horizontally away from the ExTP. It can be seen that TrPV and StPV can occasionally (about 3% of the time) extend up to  $\sim 500$  km ( $\sim 5^\circ$ , latitude) from the ExTP above the Eastern Pacific and Eastern Atlantic, indicating occasional deep horizontal tropospheric and stratospheric intrusions.

[37] We note the PDF values are much larger in the middle panels than in the right panels. This is because PDFs in the TpLat\* coordinate are occurrence probabilities at locations around the varying ExTP while PDFs in geographic latitudes are occurrence probabilities at geographic locations that can be far from the ExTP.

[38] In addition, Figure 6 shows that PDFs for these PV structures decrease with altitude. Although the maximum PDFs occur above the Eastern Pacific and the Eastern Atlantic-Mediterranean regions at and below 340 K, there is a significant frequency of PV structures at all longitudes at  $\sim 30^\circ$ N at this altitude. This global distribution is not seen at higher altitudes: There is a deep minimum (near zero in PDF) in RWB frequency above East Asia and the Northwest Pacific at 350 K and 360 K. This difference suggests more wave breaking at lower than at higher altitudes in the UTLS region [Wernli and Sprenger, 2007].

[39] Microwave Limb Sounder  $O_3$  distributions and meridional gradients in  $O_3$  abundances in TpLat\* coordinates are shown in the left and middle panels in Figure 6. To be consistent with the new TpLat\* definition, MLS  $O_3$  measurements in those tropospheric and stratospheric cutoff PV structures (see Figure 5) are left out of analysis, while MLS observations in other regions including the streamers are analyzed. This would underestimate the exchange

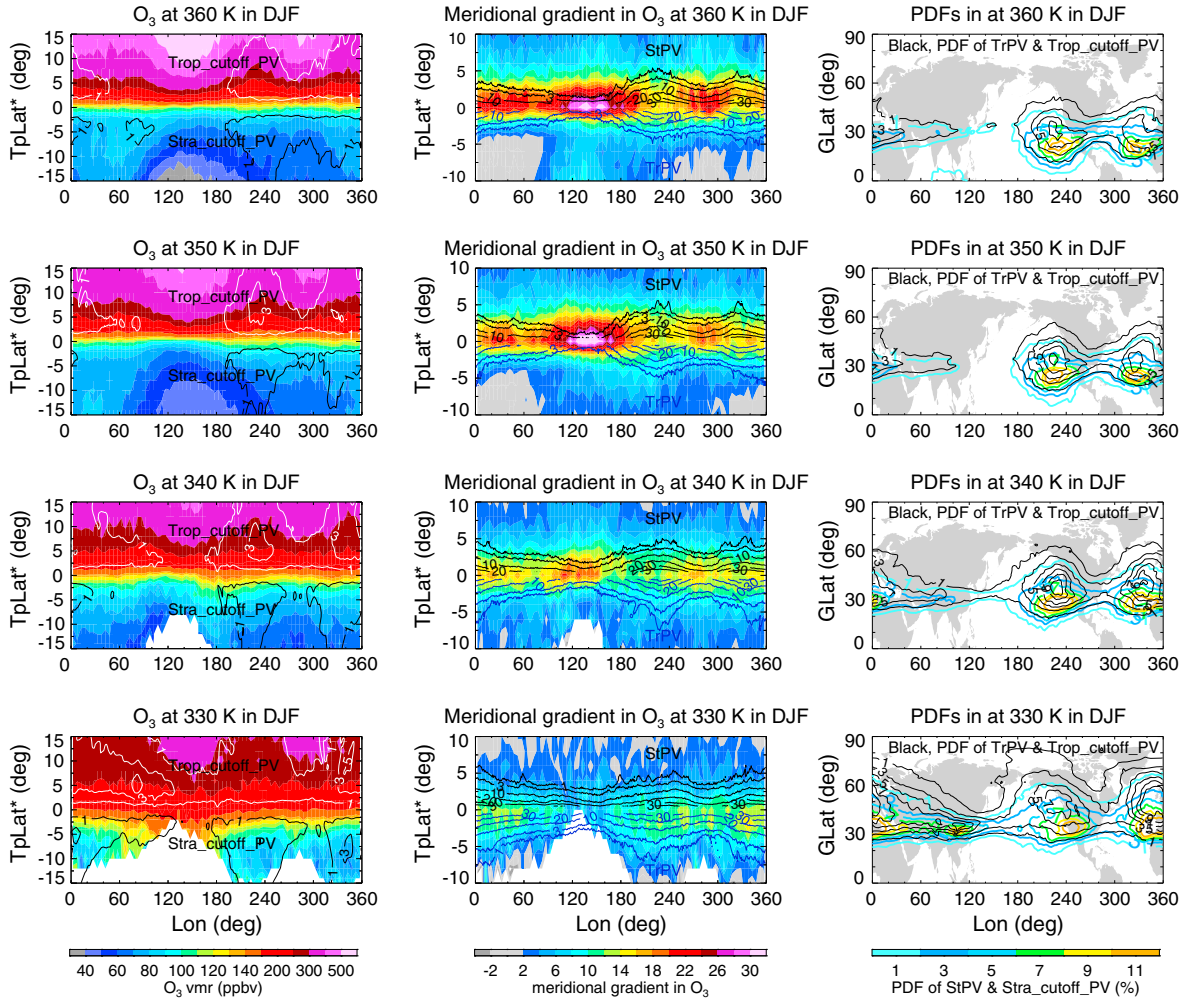


**Figure 6.** Northern hemispheric seasonal mean MLS O<sub>3</sub> distributions (panels in the left column) and meridional gradients in MLS O<sub>3</sub> (panels in the middle column) in the TpLat\* coordinate, and occurrence probabilities (PDF) of GEOS-5 tropospheric cutoff PV (Trop\_cutoff\_PV) and TrPV (black contours), and stratospheric cutoff PV (Stra\_cutoff\_PV) and StPV (color contours) in geographic latitude coordinates (panels in the right column) in NH winter (DJF). PDFs of tropospheric cutoff PV (white contours) and stratospheric cutoff PV (black contours) are also plotted in the right column. Blue and black contours in the middle column are PDFs of TrPV and StPV, respectively, in TpLat\*. PDF contour intervals are 2%, starting at 1%, in the right and left columns, while contour intervals are 1%, 3%, 10%, 20%, 30%, and 40% in the middle column. The cutoff PV contours, TrPV and StPV, are illustrated in Figure 5. TpLat\* values are determined as illustrated in Figure 5. MLS O<sub>3</sub> measurements inside the cutoff PV contours are excluded in the left and middle panels in this figure. 0° TpLat\* in this figure represents the location of the main tropopause as shown in Figure 5.

between stratosphere and troposphere, because some of the cutoff air parcels are irreversibly transported into the troposphere or stratosphere while others return to their original sphere [O'Connor *et al.*, 1999]. However, PDFs for these cutoff PV structures are small, and leaving out MLS measurements in these regions does not significantly bias this analysis. In order to account for the sharp increase of O<sub>3</sub> VMRs in the UTLS region, the gradients are calculated based on the logarithmic O<sub>3</sub> VMRs:

$$\partial \ln(\mu) / \partial \varphi = (1/\mu) (\partial \mu / \partial \varphi),$$

where  $\mu$  is O<sub>3</sub> VMR and  $\varphi$  is latitude in TpLat\* coordinates.

[40] The left panels in Figure 6 show strong zonal variations in the O<sub>3</sub> distribution in the UTLS. In the UT, relatively low

O<sub>3</sub> abundances are generally seen above the West Pacific between 340 K and 360 K, where PDFs for stratospheric cutoff PV structures are small. In the LS, relative low O<sub>3</sub> VMRs are generally seen above 240°E (120°W) longitude where PDFs for tropospheric cutoff PV structures are large. These patterns suggest that the O<sub>3</sub> distributions are influenced by RWB. We note there are high O<sub>3</sub> abundances at 330 K above East Asia and the West Pacific. It is not clear whether this enhancement of O<sub>3</sub> abundances is primarily related to RWB (consistent with the bottom-right panel in Figure 6), or to a retrieval bias at this level [Livesey *et al.*, 2011].

[41] Stratosphere-troposphere exchange pathways (barriers) are clearly demonstrated by small (large) meridional gradients in O<sub>3</sub> abundances shown in the middle panels in Figure 6. It

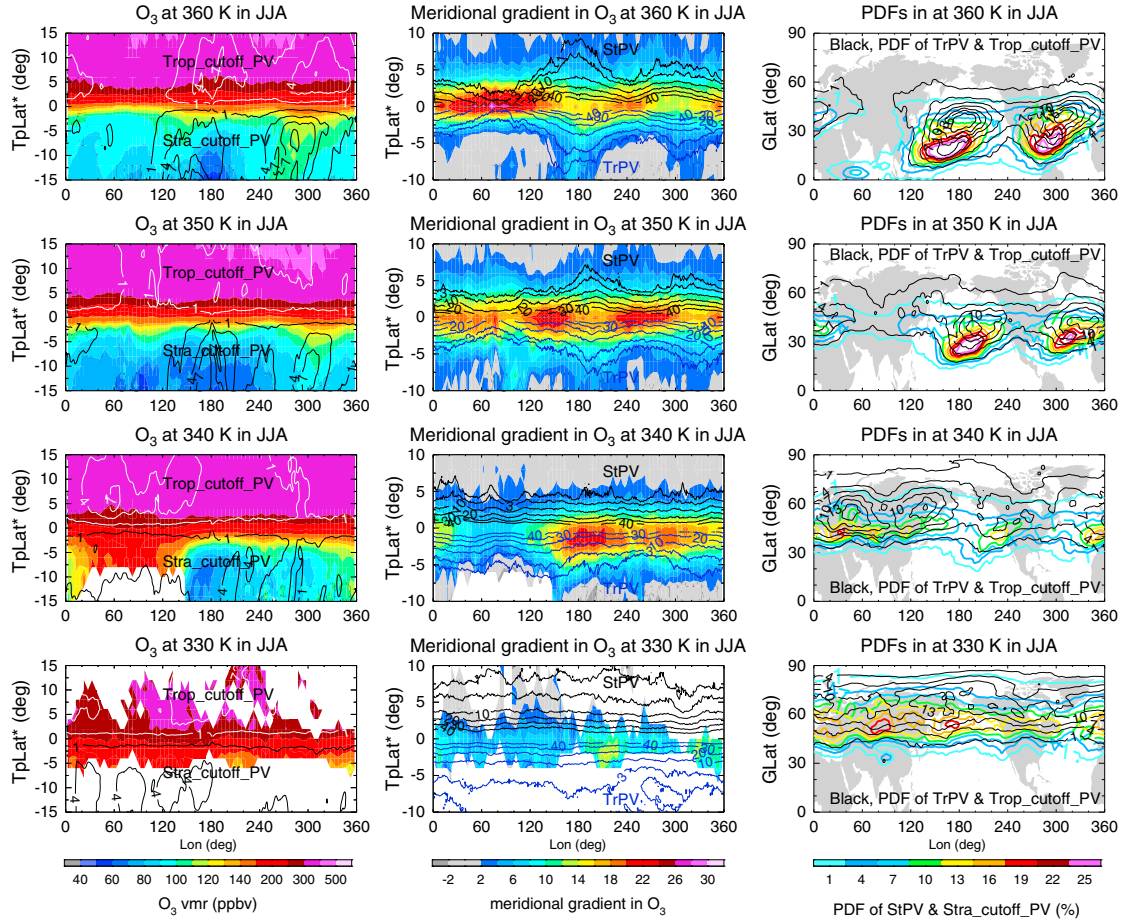


**Figure 7.** As Figure 6, but in NH summer (JJA). PDF contour intervals are 3%, starting at 1%, in the right and left columns, while the contours are 1%, 3%, 10%, 20%, 30%, and 40% in the middle column.

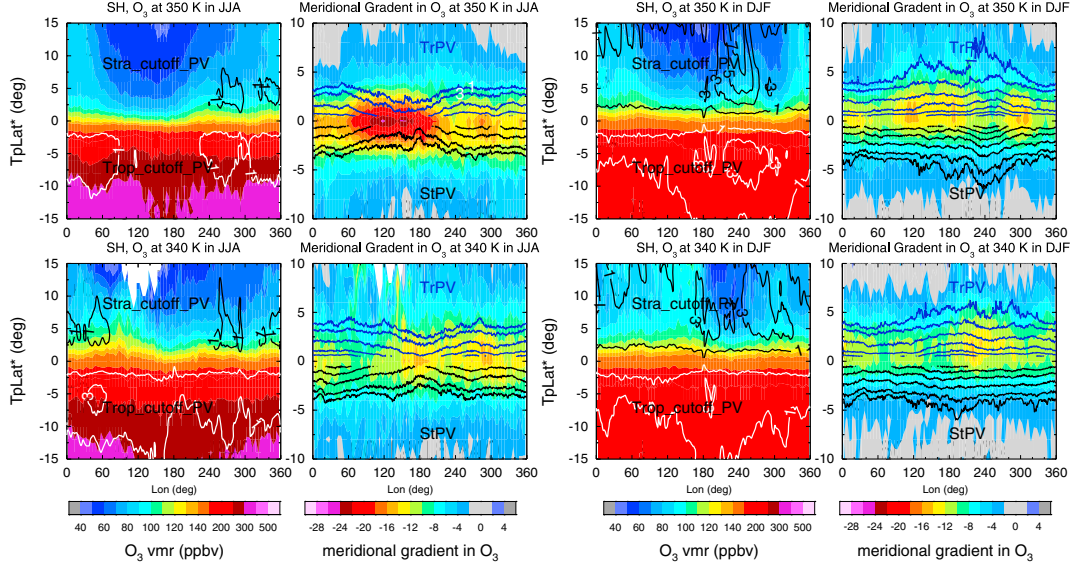


**Figure 8.** As Figures 6 and 7, but for SH at 340 K and 350 K. PDFs for PV structures in geographic latitude coordinate are not plotted. The left two columns are results in SH winter (DJF), and the right two columns are results in SH summer (JJA). The contour interval for PDFs of trop\_cutoff\_PV and stra\_cutoff\_PV is 2%, starting at 1% in the 1st and 3rd columns from the left, while the contours for PDFs of TrPV and StPV are 1%, 3%, 10%, 20%, 30%, and 40% in the 2nd and 4th columns.

shows relatively small meridional gradients in  $O_3$  around 220°E (140°W) longitude and around 330°E (30°W) longitude, suggesting strong STE in these regions between 340 K and 360 K. Large meridional gradients in  $O_3$  are seen around 140°E longitude and around 280°E (80°W) longitude, suggesting that the ExTP is a strong transport barrier in these regions, consistent with *Kunz et al.* [2011a]. This identification of the STE pathway (barrier) is supported by the co-location of large (small) PDFs of TrPV and StPV near the ExTP shown in the middle panels. We note that the STE pathways shown in Figure 6 are co-located with large Lyapunov diffusivities at middle latitudes shown by *Shuckburgh et al.* [2009], suggesting connections between wave breaking, atmospheric mixing, and STE.

[42] The relationship between the meridional  $O_3$  gradients and RWB is not as evident at 330 K as at higher levels. In fact, the middle-bottom panel shows relatively small gradients in quiescent wave-activity regions and relative large gradients in strong wave-activity regions, which is inconsistent with the view of the relationship between tracer distributions and RWB near the ExTP at higher levels. This may be due to MLS  $O_3$  retrieval bias at this level as stated above [*Livesey et al.*, 2011].

[43] Figure 7 shows the NH MLS  $O_3$  distributions, meridional gradients in these  $O_3$  abundances, and PDFs for PV structures in summer. As in winter, these distributions show strong zonal variations at levels between 340 K and 360 K. However, the locations of STE pathways and barriers vary with altitude in the summer. At 330 K, MLS measurements show large  $O_3$  abundances in the UT and small meridional gradients in them at the ExTP, but the number of observations is limited in both the UT and LS regions. Large UT  $O_3$  abundances are seen above the Eurasian region, between 0° and 150°E longitude, at 340 K. Relatively frequent RWB is also seen in this region at this level. Therefore, the high  $O_3$  VMRs in the UT at 340 K are likely due to transport from the LS [*Santee et al.*, 2011]. However, chemical production of  $O_3$  from pollution precursors over this region in summer [*Liu et al.*, 2011] is another possible contributor to enhanced  $O_3$ . UT  $O_3$  abundances are generally small between 150°E and 360°E longitude, suggesting a weaker STE effect. RWB is also slightly weaker above this region than above the Eurasian region at the altitude of 340 K, demonstrating consistency between chemical and dynamical fields.

[44] Both MLS  $O_3$  measurements and GEOS-5 PV data indicate stronger STE above the North Pacific and the North Atlantic than above the other regions at 350 K. There is strong RWB near the ExTP above the NH Pacific and Atlantic, and the strongest wave-breaking regions are above around 210°E (150°W) longitude and around 330°E (30°W) longitude at 350 K. The weakest wave-breaking regions are seen at about 80°E longitude at 350 K. Meridional gradients in  $O_3$  are in general large, and their zonal variation is small, at 350 K; however, a maximum gradient is seen at about 150°E longitude, above the Northwest Pacific, suggesting an STE barrier region there. This STE barrier is co-located with small Lyapunov diffusivity in JJA reported by *Shuckburgh et al.* [2009].

[45] The strongest wave-breaking regions on the 360 K isentropic surface are between 150°E and 210°E (150°W)

longitude and between 270°E and 330°E (between 90°W and 30°W) longitude. Relatively small gradients near the ExTP and high tropospheric  $O_3$  are seen above these regions, suggesting that they are STE pathways. These pathways are co-located with large  $O_3$  fluxes above the North Pacific and the North Atlantic at this altitude [*Jing et al.*, 2004]. Increased tropospheric  $O_3$  abundances are also seen above these regions at higher altitudes because of strong transport from the mid-latitude LS to the tropical UT in summer [*Konopka et al.*, 2010]. Very large  $O_3$  gradients are generally located above the Eurasian and North American continents where RWB is weak, suggesting the ExTP above Eurasia and North America is an STE barrier.

[46] Supplementary Figures S3 and S4 show  $O_3$  distributions and gradients in TpEqLat coordinates. Dramatic changes in  $O_3$  abundances are seen near the ExTP, along with regional variations. Separation between STE pathways and barriers, however, is not as evident in the winter as it is in the TpLat coordinate. There are large tropospheric  $O_3$  values at 340 K above the Asian region and increased tropospheric  $O_3$  abundances above the North Pacific and North Atlantic at 360 K, suggesting strong STE in these regions in summer. However, scattered large gradients in  $O_3$  near the ExTP suggest that the ExTP appears as less of a distinct transport barrier in the TpEqLat coordinate than in the TpLat coordinate.

#### 4.3. STE Pathways and Barriers in the South Hemisphere

[47] Figure 8 shows meridional gradients in  $O_3$  and PDFs of PV structures near the SH ExTP at 340 K and 350 K (see Supplementary Figure S5 for maps at 330 K–360 K). It can be seen that PDFs for PV streamers and cutoff structures have small zonal variations at 340 K in SH winter (JJA). Meridional gradients in  $O_3$  are generally small around the ExTP at this level. At higher altitudes (at and above 350 K), the PDFs have large regional variations and are significantly smaller between 80°E and 180°E than in the other regions in JJA, demonstrating regional differences in RWB near the ExTP. Weak RWB near the ExTP between 80°E and 220°E (140°W) at 350 K is associated with small STE (as evidenced in large meridional  $O_3$  gradients at the ExTP). The meridional  $O_3$  gradients are relatively small in other regions.

[48] The SH distribution of RWB in GEOS-5 is similar to that in climatologies of RWB shown in previous studies in the SH at 350 K: *Ndarana and Waugh* [2011] show that RWB near the SH ExTP is weak between 80°E and 220°E (140°W) at 350 K in JJA. These distributions are also consistent with previous studies using Lyapunov diffusivity, which is smaller near 80°E and 180°E longitude than in other regions at SH middle latitudes at 350 K in JJA [*Shuckburgh et al.*, 2009].

[49] Figure 8 also shows that RWB near the ExTP in SH is generally stronger in summer (DJF) than in winter (JJA). Meridional gradients in  $O_3$  are generally smaller in DJF than in JJA, suggesting stronger STE in summer than in winter [see also in *Santee et al.*, 2011]. Zonal variations in RWB and the meridional gradients are small at 340 K in DJF but become slightly larger at higher altitudes. The strongest RWB and smallest meridional gradients in MLS  $O_3$  are seen

above 240°E (120°W) longitude, suggesting this is the strongest STE region.

## 5. Discussion and Summary

[50] In this study, a TpLat coordinate, defined as the horizontal distance from the ExTP on isentropic surfaces, is developed to study atmospheric features near the ExTP. We demonstrate that meridional gradients in PV are extremely large at the locations of the 3.5 PVU tropopause, and these locations are generally at the center of the tropopause layer shown by the symmetric tails of meridional gradients in PV around the ExTP. Thus, we use 3.5 PVU as a reasonable definition of the ExTP. The strongest meridional gradients in PV, CO, and O<sub>3</sub> values are shown to be co-located with the ExTP. Large gradients in CO and O<sub>3</sub> abundances indicate a strong chemical discontinuity at the ExTP. This is consistent with a trajectory study [Berthet et al., 2007] that demonstrates the ExTP is a strong transport barrier between 340 K and 370 K. That study also indicates that the tropopause is more permeable below 340 K and between 370 K and 410 K, an issue not investigated here.

[51] A comparison is presented of the TpLat coordinate with the TpEqLat coordinate, which measures horizontal distances from the ExTP in EqLat [Kunz et al., 2011a]. Our study shows that chemical discontinuities using the TpLat coordinate are stronger than reported using the TpEqLat coordinate [Kunz et al., 2011a]. The fundamental issue in interpretation of TpEqLat is that it is based on the EqLat coordinate. The dynamical coordinate EqLat is useful in the stratosphere where the strong PV gradients are associated with a single simply connected jet and PV increases nearly monotonically toward the center of the polar vortex thus defined. In the UTLS, however, very large and small PV values occur near the ExTP due to the complex system of jets [Manney et al., 2011; M2013] and diabatic processes

in the UT [e.g., Pomroy and Thorpe, 2000; Grames et al., 2011]. As a result, data points geographically near the ExTP can be located far away from it in EqLat coordinates. TpEqLat-averaged chemical tracer distributions can thus be biased not only very near the ExTP but also in a broad UTLS region as shown in this study and as discussed by Manney et al. [2011] and Pan et al. [2012]. However, Figure 4 demonstrates TpEqLat (or EqLat) is more useful for revealing the diabatic STE processes for the reason discussed above. Therefore, TpLat and TpEqLat can be complementary tools in UTLS studies.

[52] Figure 9 shows NH GEOS-5 wind (U) and PV distributions in TpLat\* coordinate in winter and summer. TpLat\* is a modification of TpLat and is determined as shown in Figure 5, with 0° TpLat\* at the location of the main ExTP. Figure 9 shows that the subtropical jet strength is dramatically reduced between winter and summer. By contrast, seasonal mean PV gradients are slightly larger at the ExTP in summer than in winter. We note that strong RWB activity in summer, which is related to the weak subtropical jet, reduces PV gradients at the ExTP [Haynes and Shuckburgh, 2000a]. However, tropopause foldings in RWBs can result in large PV gradients near the ExTP before they break [e.g., Holton et al., 1995; Haynes et al., 2001] and can compensate for the reduction in those gradients due to RWB in these seasonal mean PV fields in the TpLat coordinate. We also note that static stability is slightly stronger above the ExTP in summer than in winter [Birner, 2006; Randel et al., 2007; Grise et al., 2010], consistent with the relationship between meridional PV gradients and meridional gradients in static stability [Birner, 2006]. Nevertheless, this figure suggests that the relationship between global mean PV gradients and RWB activity near the ExTP is complex. Figure 9 shows the jet core is typically between 340 K and 350 K at 0° TpLat\* in both winter and summer [Kunz et al., 2011b; Manney et al., 2011, and references therein]. As shown in Figure 3c, the co-location of 0° TpLat\* and jet core

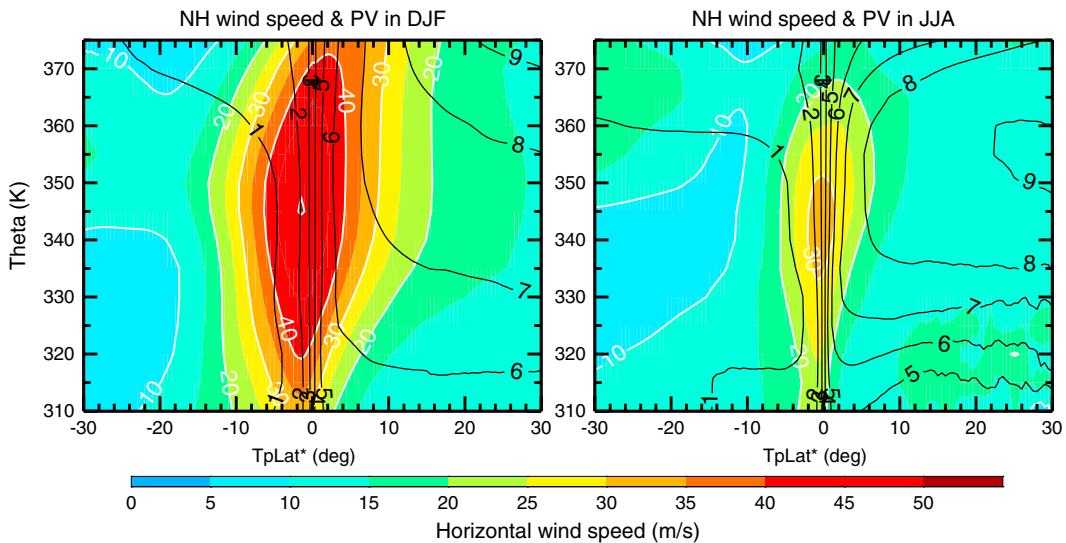


**Figure 9.** NH seasonal mean GEOS-5 horizontal wind speed (U and V, shaded in color, and white contours) and potential vorticity (black contours, in PVU) in the UTLS in TpLat\* coordinate in winter (DJF) and summer (JJA). TpLat\* values are determined as illustrated in Figure 5, and data in the cutoff PV contours (see Figure 5) are not included.

indicates consistency between the tropopause coordinate and the jet coordinate introduced by *Manney et al.* [2011] at these altitudes wherever the latter is well defined.

[53] Microwave Limb Sounder CO retrievals have coarse vertical resolution, about 3–4 km, in the UTLS region, thus have broad averaging kernels [Livesey *et al.*, 2011]. These broad averaging kernels smooth the atmospheric tracer profiles in retrievals. Therefore, it is expected that the chemical discontinuities shown here at the ExTP would be even stronger if MLS measurements had higher vertical resolution.

[54] The distributions of RWB in our analysis are consistent with those in previous reports [*Postel and Hitchman*, 1999; *Wernli and Sprenger*, 2007; *Hitchman and Huesmann*, 2007; *Nadarana and Waugh*, 2011]. However, RWB frequencies near the ExTP in the tropopause latitude coordinate shown in this study are much larger than those in previous reports, because application of the coordinate makes the statistics focus on the regions always near the varying tropopause.

[55] Meridional gradients in MLS O<sub>3</sub> and RWB statistics derived from GEOS-5 PV structures show that NH STE pathways are mainly located above the Eastern Pacific and above the Atlantic-Mediterranean region in NH winter (Dec–Jan–Feb). The NH pathways spread globally at 330 K in summer (Jun–Jul–Aug). However, they are mainly located above western Asia at 340 K, and above the Atlantic and the center North Pacific at 350 K and 360 K in summer. There are strong transport barriers above Eastern Asia and the Western Pacific and above North America at these altitudes in winter, and these barriers move westward in summer. Generally, the zonal variation in southern hemispheric STE is small at and below 340 K. However, the ExTP is a strong barrier above the Eastern Indian Ocean and the Southwestern Pacific at and above 350 K in SH winter, and there is strong STE above the Southeastern Pacific at these levels during SH summer.

[56] **Acknowledgments.** We thank John (Jack) C. McConnell for useful conversation and three reviewers for helpful comments. Work at Jet Propulsion Laboratory, California Institute of Technology was done under contract with the National Aeronautics and Space Administration (NASA). GEOS-5 data used in this study were provided by the Global Modeling and Assimilation Office (GMAO) at NASA Goddard Space Flight Center through the NASA GES DISC online archive.

## References

- Allen, D. R., *et al.* (1999), Observations of middle atmosphere CO from the UARS ISAMS during the early northern winter 1991/92, *J. Atmos. Sci.*, **56**, 563–583.
- Ambaum, M. (1997), Isentropic formation of the tropopause, *J. Atmos. Sci.*, **54**, 555–568.
- Appenzeller, C., J. R. Holton, and K. H. Rosenlof (1996a), Seasonal variation of mass transport across the tropopause, *J. Geophys. Res.*, **101**, 15,071–15,078.
- Appenzeller, C., H. C. Davies, and W. A. Norton (1996b), Fragmentation of stratospheric intrusions, *J. Geophys. Res.*, **101**, 1435–1456.
- Bethan, S., G. Vaughan, and S. J. Reid (1996), A comparison of ozone and thermal tropopause heights and the impact of tropopause definition on quantifying the ozone content of the troposphere, *Q. J. R. Meteorol. Soc.*, **122**, 929–944, doi:10.1002/qj.49712253207.
- Berthet, G., J. G. Esler, and P. H. Haynes (2007), A Lagrangian perspective of the tropopause and the ventilation of the lowermost stratosphere, *J. Geophys. Res.*, **112**, D18102, doi:10.1029/2006JD008295.
- Birner, T., A. Dörnbrack, and U. Schumann (2002), How sharp is the tropopause at midlatitudes?, *Geophys. Res. Lett.*, **29**(14), 1700, doi:10.1029/2002GL015142.
- Birner, T. (2006), Fine-scale structure of the extratropical tropopause region, *J. Geophys. Res.*, **111**, D04104, doi:10.1029/2005JD006301.
- Bithell, M., L. J. Gray, and B. D. Cox (1999), A three-dimensional view of the evolution of midlatitude stratospheric intrusions, *J. Atmos. Sci.*, **56**(5), 673–688.
- Bloom, S. C., L. L. Takacs, A. M. da Silva, and D. Ledvina (1996), Data assimilation using incremental analysis updates, *Mon. Wea. Rev.*, **124**, 1256–1271.
- Butchart, N., and E. E. Remsberg (1986), The area of the stratospheric polar vortex as a diagnostic for tracer transport on an isentropic surface, *J. Atmos. Sci.*, **43**, 1319–1339.
- Chen, P. (1995), Isentropic cross-tropopause mass exchange in the extratropics, *J. Geophys. Res.*, **100**(D8), 16,661–16,673, doi:10.1029/95JD01264.
- Fischer, H., *et al.* (2000), Tracer correlations in the northern high latitude lowermost stratosphere: Influence of cross-tropopause mass exchange, *Geophys. Res. Lett.*, **27**(1), 97–100, doi:10.1029/1999GL010879.
- Fueglistaler, S., *et al.* (2009), Tropical tropopause layer, *Rev. Geophys.*, **47**, RG1004, doi:10.1029/2008RG000267.
- Gettelman, A., *et al.* (2011), The extra tropical upper troposphere and lower stratosphere, *Rev. Geophys.*, doi:10.1029/2011RG000355.
- Grams, C. M., H. Wernli, M. Böttcher, J. Čampa, U. Corsmeier, S. C. Jones, J. H. Keller, C.-J. Lenz and L. Wiegand (2011), The key role of diabatic processes in modifying the upper-tropospheric wave guide: A North Atlantic case-study, *Q.J.R. Meteorol. Soc.*, **137**, 2174–2193, doi:10.1002/qj.891.
- Grise, K. M., D. W. J. Thompson, and T. Birner (2010), A global survey of static stability in the stratosphere and upper troposphere, *J. Clim.*, **23**, 2275–2292.
- Haynes, P., and E. Shuckburgh (2000a), Effective diffusivity as a diagnostic of atmospheric transport: 1. Stratosphere, *J. Geophys. Res.*, **105**(D18), 22777–22794, doi:10.1029/2000JD900093.
- Haynes, P., and E. Shuckburgh (2000b), Effective diffusivity as a diagnostic of atmospheric transport: 2. Troposphere and lower stratosphere, *J. Geophys. Res.*, **105**(D18), 22,795–22,810.
- Haynes, P., J. Scinocca, and M. Greenslade (2001), Formation and maintenance of the extratropical tropopause by baroclinic eddies, *Geophys. Res. Lett.*, **28**(22), doi:10.1029/2001GL013485.
- Hegglin, M. I., and T. G. Shepherd (2009), Large climate-induced changes in ultraviolet index and stratosphere-to-troposphere ozone flux, *Nat. Geosci.*, **2**, 687–691.
- Hegglin, M. I., D. Brunner, T. Peter, J. Staehelin, V. Wirth, P. Hoor, and H. Fischer (2005), Determination of eddy diffusivity in the lowermost stratosphere, *Geophys. Res. Lett.*, **32**, L13812, doi:10.1029/2005GL022495.
- Hegglin, M. I., *et al.* (2006), Measurements of NO, NO<sub>y</sub>, N<sub>2</sub>O and O<sub>3</sub> during spurt: Implications for transport and chemistry in the lowermost stratosphere, *Atmos. Chem. Phys.*, **6**, 1331–1350.
- Hegglin, M. I., *et al.* (2009), A global view of the extratropical tropopause transition layer from Atmospheric Chemistry Experiment Fourier Transform Spectrometer O<sub>3</sub>, H<sub>2</sub>O, and CO, *J. Geophys. Res.*, **114**, D00B11, doi:10.1029/2008JD009984.
- Highwood, E. J., B. J. Hoskins, and P. Berrisford (2000), Properties of the arctic tropopause, *Q. J. R. Meteorol. Soc.*, **126**, 1515–1532.
- Hitchman, M. H., and A. S. Huesmann (2007), A seasonal climatology of Rossby wave breaking in the 320–2000-K layer, *J. Atmos. Sci.*, **64**, 1922–1940.
- Hoerling, M. P., T. K. Schaack, and A. J. Lenzen (1991), Global objective tropopause analysis, *Mon. Wea. Rev.*, **119**, 1816–1831.
- Holton, J. R., *et al.* (1995), Stratosphere-troposphere exchange, *Rev. Geophys.*, **33**(4), 403–439.
- Homeyer, C. R., K. P. Bowman, L. L. Pan, E. L. Atlas, R.-S. Gao, and T. L. Campos (2011), Dynamical and chemical characteristics of tropospheric intrusions observed during START08, *J. Geophys. Res.*, **116**, D06111, doi:10.1029/2010JD015098.
- Hoor, P., H. Fischer, L. Lange, J. Lelieveld, and D. Brunner (2002), Seasonal variations of a mixing layer in the lowermost stratosphere as identified by the CO-O<sub>3</sub> correlation from in situ measurements, *J. Geophys. Res.*, **107**, 4044, doi:10.1029/2000JD000289.
- Hoor, P., H. Wernli, M. I. Hegglin, and H. Bönisch (2010), Transport timescales and tracer properties in the extratropical UTLS, *Atmos. Chem. Phys.*, **10**, 7929–7944.
- Hoskins, B. J., M. E. McIntyre, and A. W. Robertson, (1985), On the use and significance of isentropic potential vorticity maps, *Quart. J. Roy. Meteor. Soc.*, **111**, 877–946.
- Hsu, J., M. J. Prather, and O. Wild (2005), Diagnosing the stratosphere-to-troposphere flux of ozone in a chemistry transport model, *J. Geophys. Res.*, **110**, D19305, doi:10.1029/2005JD006045.
- Jiang, J. H., *et al.* (2007), Connecting surface emissions, convective uplifting, and long-range transport of carbon monoxide in the upper

- troposphere: New observations from the Aura Microwave Limb Sounder, *Geophys. Res. Lett.*, 34, L18812, doi:10.1029/2007GL030638.
- Jin, J. J., et al. (2009), Comparison of CMAM simulations of carbon monoxide (CO), nitrous oxide ( $N_2O$ ), and methane ( $CH_4$ ) with observations from Odin/SMR, ACE-FTS, and Aura/MLS, *Atmos. Chem. Phys.*, 9, 3233–3252.
- Jing, P., D. M. Cunnold, H. J. Wang, E-S. Yang (2004), Isentropic cross-tropopause ozone transport in the Northern Hemisphere, *J. Atmos. Sci.*, 61, 1068–1078.
- Konopka, P., et al. (2010), Annual cycle of ozone at and above the tropical tropopause: Observations versus simulations with the Chemical Lagrangian Model of the Stratosphere (CLaMS), *Atmos. Chem. Phys.*, 10, 121–132, doi:10.5194/acp-10-121-2010.
- Krebsbach, M., C. Schiller, D. Brunner, G. Günther, M. I. Hegglin, D. Mottaghy, M. Riese, N. Spelten, and H. Wernli (2006), Seasonal cycles and variability of  $O_3$  and  $H_2O$  in the UT/LMS during SPURT, *Atmos. Chem. Phys.*, 6, 109–125.
- Kunz, A., L. L. Pan, P. Konopka, D. E. Kinnison, and S. Tilmes (2011a), Chemical and dynamical discontinuity at the extratropical tropopause based on START08 and WACCM analyses, *J. Geophys. Res.*, 116, D24302, doi:10.1029/2011JD016686.
- Kunz, A., P. Konopka, R. Müller, and L. L. Pan (2011b), Dynamical tropopause based on isentropic potential vorticity gradients, *J. Geophys. Res.*, 116, D01110, doi:10.1029/2010JD014343.
- Li, Q., et al. (2005), North American pollution outflow and the trapping of convectively lifted pollution by upper-level anticyclone, *J. Geophys. Res.*, 110, D10301, doi:10.1029/2004JD005039.
- Lin, S.-J., (2004): A vertically Lagrangian finite-volume dynamical core for global models, *Mon. Wea. Rev.*, 132, 2293–2307.
- Liu, J. J., D. B. A. Jones, S. Zhang, and J. Kar (2011), Influence of interannual variations in transport on summertime abundances of ozone over the Middle East, *J. Geophys. Res.*, 116, D20310, doi:10.1029/2011JD016188.
- Livesey, N. J., et al. (2008), Validation of Aura Microwave Limb Sounder  $O_3$  and CO observations in the upper troposphere and lower stratosphere, *J. Geophys. Res.*, 113, D15S02, doi:10.1029/2007JD008805.
- Livesey, N. J., et al. (2011), Version 3.3 level 2 data quality and description document, Tech. Rep. JPL-D-3509, Jet Propul. Lab., Pasadena, Calif. (Available from <http://mls.jpl.nasa.gov>.)
- Logan, J. A. (1999), An analysis of ozonesonde data for the troposphere: Recommendations for testing 3-D models and development of a gridded climatology for tropospheric ozone, *J. Geophys. Res.*, 104(D13), 16,115–16,149, doi:10.1029/1998JD100096.
- Manney, G. L., et al. (2007), Solar occultation satellite data and derived meteorological products: Sampling issues and comparisons with Aura MLS, *J. Geophys. Res.*, 112, D24S50, doi:10.1029/2007JD008709.
- Manney, G. L., et al. (2008) The evolution of the stratopause during the 2006 major warming: Satellite data and assimilated meteorological analyses. *J. Geophys. Res.*, 113, D11115.
- Manney, G. L., et al. (2011), Jet characterization in the upper troposphere/lower stratosphere (UTLS): Applications to climatology and transport studies, *Atmos. Chem. Phys.*, 11, 6115–6137.
- Manney, G. L., H. A. Michelsen, M. L. Santee, M. R. Gunson, F. W. Irion, A. E. Roche, and N. J. Livesey (1999), Polar vortex dynamics during spring and fall diagnosed using trace gas observations from the Atmospheric Trace Molecule Spectroscopy instrument, *J. Geophys. Res.*, 104, 18,841–18,866.
- Manney, G. L., et al. (2009), Aura Microwave Limb Sounder observations of dynamics and transport during the record-breaking 2009 Arctic stratospheric major warming, *Geophys. Res. Lett.*, 36, doi:10.1029/2009GL038586.
- Martius, O., C. Schwierz, and H. C. Davies (2010), Tropopause-level wave-guides. *J. Atmos. Sci.*, 67, 866–879.
- Nadarana, T., and D. W. Waugh (2011), A climatology of Rossby wave breaking on the southern hemisphere tropopause, *J. Atmos. Sci.*, 68, 798–811.
- O'Connor, F. M., G. Vaughan, and H. De Backer (1999), Observations of subtropical air in the European mid-latitude lower stratosphere, *Quart. J. Roy. Meteor. Soc.*, 125, 2965–2986.
- Olsen, M. A., A. R. Douglass, P. A. Newman, J. C. Gille, B. Nardi, V. A. Yudin, D. E. Kinnison, and R. Khosravi (2008), HIRDLS observations and simulation of a lower stratospheric intrusion of tropical air to high latitudes, *Geophys. Res. Lett.*, 35, L21813, doi:10.1029/2008GL035514.
- Pan, L. L., et al. (2004), Definitions and sharpness of the extratropical tropopause: A trace gas perspective, *J. Geophys. Res.*, 109, D23103, doi:10.1029/2004JD004982.
- Pan, L. L., et al. (2012), Commentary on using equivalent latitude in the upper troposphere and lower stratosphere, *Atmos. Chem. Phys.*, 12, 9187–9199.
- Pan, L. L., J. C. Wei, D. E. Kinnison, R. R. Garcia, D. J. Wuebbles, and G. P. Brasseur (2007), A set of diagnostics for evaluating chemistry-climate models in the extratropical tropopause region, *J. Geophys. Res.*, 112, D09316, doi:10.1029/2006JD007792.
- Park, M., W. J. Randel, L. K. Emmons, and N. J. Livesey (2009), Transport pathways of carbon monoxide in the Asian summer monsoon diagnosed from Model of Ozone and Related Tracers (MOZART), *J. Geophys. Res.*, 114, D08303, doi:10.1029/2008JD010621.
- Pawson, S., et al. (2007), Stratospheric transport using six-hour averaged winds from a data assimilation system, *J. Geophys. Res.*, 112, D23103, doi:10.1029/2006JD007673.
- Polvani, L. M., and J. G. Esler (2007), Transport and mixing of chemical air masses in idealized baroclinic life cycles, *J. Geophys. Res.*, 112, D23102, doi:10.1029/2007JD008555.
- Pomroy, H. R., and A. J. Thorpe (2000), The evolution and dynamical role of reduced upper-tropospheric potential vorticity in intensive observing period one of FASTEX, *Mon. Wea. Rev.*, 128, 1817–1834.
- Postel, G. A., and M. H. Hitchman (1999), A climatology of Rossby wave breaking along the subtropical tropopause, *J. Atmos. Sci.*, 56, 359–373.
- Prather, M. J., et al. (2011), An atmospheric chemist in search of the tropopause, *J. Geophys. Res.*, 116, D04306, doi:10.1029/2010JD014939.
- Randel, W. J., F. Wu, and P. Forster (2007), The extratropical tropopause inversion layer: Global observations with GPS data, and a radiative forcing mechanism, *J. Atmos. Sci.*, 64, 4489–4496.
- Randel, W. J., M. Park, L. Emmons, D. Kinnison, P. Bernath, K. A. Walker, C. Boone, and H. Pumphrey (2010), Asian monsoon transport of pollution to the stratosphere, *Science*, 328, 611–613, doi:10.1126/science.1182274.
- Ray, E. A., et al. (2004), Distributions of ozone in the region of the subtropical jet: An analysis of in situ aircraft measurements, *J. Geophys. Res.*, 109, D08106, doi:10.1029/2003JD004143.
- Reed, R. J. (1955), A study of a characteristic type of upper-level frontogenesis, *J. Meteorol.*, 12, 226–237.
- Rienecker, M. M., et al. (2008), The GEOS-5 data assimilation system—Documentation of versions 5.0.1 and 5.1.0, and 5.2.0. NASA Tech. Rep. Series on Global Modeling and Data Assimilation, NASA/TM-2008-104606, Vol. 27, 92 pp.
- Santee, M. L., G. L. Manney, N. J. Livesey, L. Froidevaux, M. J. Schwartz, and W. G. Read (2011), Trace gas evolution in the lowermost stratosphere from Aura Microwave Limb Sounder measurements, *J. Geophys. Res.*, 116, D18306, doi:10.1029/2011JD015590.
- Schoeberl, M. R. (2004), Extratropical stratosphere-troposphere mass exchange, *J. Geophys. Res.*, 109, D13303, doi:10.1029/2004JD004525.
- Schoeberl, M. R., B. N. Duncan, A. R. Douglass, J. Waters, N. Livesey, W. Read, and M. Filippiak (2006), The carbon monoxide tape recorder, *Geophys. Res. Lett.*, 33, L12811, doi:10.1029/2006GL026178.
- Scott, R. K., E. F. Shuckburgh, J.-P. Cammas, and B. Legras (2003), Stretching rates and equivalent length near the tropopause, *J. Geophys. Res.*, 108(D13), 4394, doi:10.1029/2002JD002988.
- Shepherd, T. G. (2002), Issue in stratosphere-troposphere coupling, *J. of the Meteo. Soc. of Japan*, 80(4B), 769–792.
- Shuckburgh, E., F. d'Ovidio, and B. Legras (2009), Local mixing events in the upper troposphere and lower stratosphere. Part II: Seasonal and interannual variability, *J. Atmos. Sci.*, 66(12), 3695, doi:10.1175/2009JAS2983.1.
- Solomon, S., K. H. Rosenlof, R. W. Portmann, J. S. Daniel, S. M. Davis, T. J. Sanford, and G-K. Plattner (2010), Contributions of stratospheric water vapor to decadal changes in the rate of global warming, *Science*, 327, 1219–1223, doi:10.1126/science.1182488.
- Sprenger, M., and H. Wernli (2003), A northern hemispheric climatology of cross-tropopause exchange for the ERA15 time period (1979–1993), *J. Geophys. Res.*, 108, 8521, doi:10.1029/2002JD002636.
- Sprenger, M., H. Wernli, and Michel Bourqui (2007), Stratosphere-troposphere exchange and its relation to potential vorticity streamers and cutoffs near the extratropical tropopause, *J. Atmos. Sci.*, 64, 1587–1602.
- Stohl, A. (2001), A 1-year Lagrangian “climatology” of airstreams in the Northern Hemisphere troposphere and lowermost stratosphere, *J. Geophys. Res.*, 106, 7263–7279.
- Stohl, A., et al. (2003), Stratosphere-troposphere exchange: A review, and what we have learned from STACCATO, *J. Geophys. Res.*, 108, 8516, doi:10.1029/2002JD002490.
- Strahan, S. E., B. N. Duncan, and P. Hoor (2007), Observationally derived transport diagnostics for the lowermost stratosphere and their application to the GMI chemistry and transport model, *Atmos. Chem. Phys.*, 7, 2435–2445, doi:10.5194/acp-7-2435-2007.
- Tilmes, S., et al. (2010), An aircraft-based upper troposphere lower stratosphere  $O_3$ , CO, and  $H_2O$  climatology for the Northern Hemisphere, *J. Geophys. Res.*, 115, D14303, doi:10.1029/2009JD012731.
- Vogel, B., et al. (2011), Transport pathways and signatures of mixing in the extratropical tropopause region derived from Lagrangian model simulations, *J. Geophys. Res.*, 116, D05306, doi:10.1029/2010JD014876.

- Wargan, K., S. Pawson, I. Stajner, and V. Thouret (2010), Spatial structure of assimilated ozone in the upper troposphere and lower stratosphere, *J. Geophys. Res.*, 115, D24316, doi:10.1029/2010JD013941.
- Waugh, D. W., and B. M. Funatsu (2003), Intrusions into the tropical upper troposphere: Three dimensional structure and accompanying ozone and OLR distributions, *J. Atmos. Sci.*, 60, 637–653.
- Wernli, H., and M. Bourqui (2002), A Lagrangian “1-year climatology” of (deep) cross-tropopause exchange in the extratropical Northern Hemisphere, *J. Geophys. Res.*, 107(D2), 4021, doi:10.1029/2001JD000812.
- Wernli, H., and M. Sprenger (2007), Identification and ERA-15 climatology of potential vorticity streamers and cutoffs near the extratropical tropopause, *J. Atmos. Sci.*, 64, 1569–1586.
- World Meteorological Organization (WMO) (1995), Manual on codes: International codes, vol. I.1, part A, WMO-No. 306, Geneva, Switzerland.
- Zahn, A., and C. A. M. Brenninkmeijer (2003), New directions: A chemical tropopause defined, *Atmos. Environ.*, 37(3), 439–440, doi:10.1016/S1352-2310(02)00901-9.